JTTEE5 19:317–327
DOI: 10.1007/s11666-009-9450-y
1059-9630/$19.00 © ASM International

Elaboration of Porous NiO/8YSZ Layers by Several SPS and SPPS Routes

Pierrette Michaux, Ghislain Montavon, Alain Grimaud, Alain Denoirjean, and Pierre Fauchais

(Submitted April 23, 2009; in revised form August 28, 2009)

Solution Precursor Plasma Spraying (SPPS) is a thermal spray process where a feedstock solution is heated and pyrolized to form fine (i.e., ≪1000 nm) molten particles that deposit onto a substrate to form a layer. The benefits of implementing the SPPS process include, among others: (i) the possibility to create unique microstructures at nanometer scale without the injection feeding problems usually associated to powder feeders and delivery cables and (ii) rapid exploration of novel precursor compositions. In this study, preparation and characterization of porous anode layers with homogeneous Nickel distribution and nanometer sized microstructure are considered for solid oxide fuel cell (SOFC) application. Once the solution is injected, the droplets go through several chemical and physical changes and impact the substrate in different states, from fully molten one to unpyrolized one. The effects of some spray parameters, such as the spray distance and the plasma flow mass enthalpy, on the layer architecture and composition were investigated. The results show that dense or porous layers can be manufactured depending on the operating parameters.

Keywords anode, fuel Cells, NiO/YSZ, Solution Precursor Plasma Spraying, suspension plasma spraying

1. Introduction

Solid oxide fuel cells (SOFCs) include in their design an anode layer made usually of cermet layer of nickel and yttria-stabilized zirconia (YSZ) through which hydrogen species permeate. This layer needs to fulfill several characteristics among which: (i) a controlled void network architecture ensuring the appropriate permittivity factor, (ii) an adequate Ni over YSZ volume fraction, and (iii) a fine dispersion of YSZ among Ni to limit to the maximum possible extend sintering during operation (Ref 1).

Several manufacturing routes can be implemented to achieve this functional layer, among which thermal spraying appears as one of the most pertinent thanks to its versatility and flexibility (Ref 2-4).

Conventional atmospheric plasma spraying (APS) is limited to the injection of powders with a typical range between 10 and 100 μm (Ref 5, 6). This leads to a limitation in term of layer microstructure and its related electrochemical reactivity. Decreasing the size of the precursors permits to improve the layer performances thanks to a finer structure and porous architecture allowing a higher reactive rate between nickel and hydrogen species (Ref 3).

One possible route aims at spraying micrometer-sized agglomerates of nanometer-sized nickel mono-oxide and YSZ (Ref 4) particles. Beside the sharpened carcinogen character of nickel mono-oxide (Ref 7), layers manufactured via this route exhibit a two-scale structure, nanometer- and micrometer-sized, corresponding to particle cores that were not molten within the plasma flow and particle peripheral areas that were molten, respectively (Ref 8). Such a structure, usually typified as ''bimodal'', impedes the layer functional properties by decreasing its mechanical and reactive properties.

Another possible route relies in Solution Precursor Plasma Spraying (SPPS) where chemical precursors are injected into the plasma jet. Jordan et al. manufactured YSZ thermal barrier coatings by spraying precursor salts containing zirconium and yttrium (Ref 9-13). Whereas nothing about synthesis of cermet layers by SPPS process has been found in the literature, a few articles related to the synthesis of NiO-YSZ particles by spray pyrolysis have been identified (Ref 14, 15).

This article aims at presenting on-going research works carried-out to manufacture NiO/8YSZ layers exhibiting nanometer-sized architectures in view of improving functional performances of SOFC anodes. SPPS and suspension plasma spraying (SPS) were considered as the manufacturing routes. In this latter case, a composite powder has been synthesized by impregnation of zirconia sub-micrometer-sized particles by a Ni salt.

This article is an invited paper selected from presentations at the 2009 International Thermal Spray Conference and has been expanded from the original presentation. It is simultaneously published in *Expanding Thermal Spray Performance to New Markets and Applications: Proceedings of the 2009 International Thermal Spray Conference*, Las Vegas, Nevada, USA, May 4-7, 2009, Basil R. Marple, Margaret M. Hyland, Yuk-Chiu Lau, Chang-Jiu Li, Rogerio S. Lima, and Ghislain Montavon, Ed., ASM International, Materials Park, OH, 2009.

Pierrette Michaux, Ghislain Montavon, Alain Grimaud, Alain Denoirjean, and **Pierre Fauchais**, Faculty of Sciences and Technologies, SPCTS, UMR CNRS 6638, University of Limoges, 123 Avenue Albert Thomas, 87060 Limoges cedex, France. Contact e-mail: ghislain.montavon@unilim.fr.

Effects of some operating parameters (spray distance, plasma flow mass enthalpy, etc.) on the layer architecture and its composition were investigated. These parameters appear more critical in the SPPS process compared to SPS one (Ref 8, 16) since a chemical precipitation should take place in the time of only a few tenths of millisecond of reaction.

2. Experimental Procedures

Two different processes were considered to manufacture those layers: (i) SPS using a suspension of NiO/8YSZ nanometer-sized particles synthesized by chemical route and (ii) SPPS using a mixture of raw salts of components in the appropriate molar fractions.

2.1 SPPS Process

Figure 1 presents a schematic of the experimental system. The precursor solution is stored in a pressurized container at about 0.5 MPa and goes through an injector of internal diameter $d_0 = 150$ μm at a velocity of about 22 m/s. At the injector exit, a stream is generated and injected in the plasma flow where rapid fragmentation followed by evaporation occur (Ref 9). This step is followed by precipitation, pyrolysis, and melting of products to form fine (i.e., $\ll$1000 nm) particles that impact the substrate to form a layer. Depending upon the plasma jet region where droplets travel, core or fringes, melted or non-pyrolized particles, respectively, are embedded in the layers (Ref 11). This process requires, hence to carefully controlling experimental conditions (solution concentration, substrate preheating, plasma gases powder, etc.) to avoid inclusion of defects during coating formation. Non-cohesive coating, delamination between two coatings and cracks are the most frequently encountered defects in plasma spraying (Ref 17, 18).

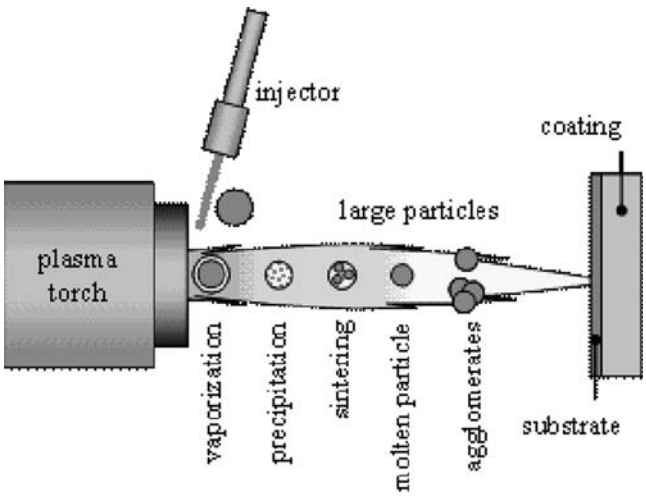

Fig. 1 SPPS process

2.2 SPS Process

The principle of SPS process is somewhat the same than SPPS except that the stream injected in the plasma flow is an alcoholic suspension elaborated from NiO/8YSZ synthesized powders. Power and injection parameters were optimized in previous work (Ref 16, 19). Therefore, first experiment was realized at a spray distance of 40 mm under an Ar-H_2 plasma gas mixture (Table 1).

2.3 Precursors

2.3.1 SPS Precursors. NiO/8YSZ composite particles were prepared by chemical route (Ref 20-22) impregnating 8YSZ powder (Unitec Ceramics, Stafford, UK) of particle size distribution ranging from 100 (d_{10}) to 1200 (d_{90}) nm with an average size of 400 nm (d_{50}), with an aqueous solution of nickel acetate $Ni(CH_3COO)_2{\cdot}4H_2O$ precursor (Alfa Aesar GmbH, Schiltigheim, France). The resulting slurry was heated to about 100 °C under continuous stirring until all the water evaporated. The solid residue, once crushed in a mortar, was calcined at 500 °C for 2 h, in order to remove all organic components in the final powder. The NiO loading of the composite powder thus prepared was 50 vol.%. For injection in the plasma flow, a 10 wt.% suspension was prepared in Et-OH (99.5%).

2.3.2 SPPS Precursors. The solution was formulated by dissolving nickel ($Ni(NO_3)_2$), yttrium ($Y(NO_3)_3$), and zirconyl ($ZrO(NO_3)_2$) nitrates in a solvent (Et-OH, 99.5%) at fractions to result in a 50 vol.% Ni/8 mol.% Y_2O_3-ZrO_2 ceramic solid solution in the layer.

2.4 Spray Operating Parameters

A stick mono-cathode plasma torch ($P_{elec.} \sim 50$ kW) developed in house and equipped with a 6 mm internal diameter nozzle was used to manufacture the layers. This torch is equipped with a thoried tungsten cathode whereas the anode is made of pure electrolytic copper. Plasma gas mixture is injected axially upstream the electric arc chamber. The system is cooled down by pressurized water and its thermal efficiency is in the order of 60%. The power and injection parameters are summarized in Table 1. Effects of spray distance, plasma flow mass enthalpy, and plasma forming gas mixture on layer architecture and composition were investigated. Solution/suspension injection parameters were adjusted accordingly

Table 1 Power and injection parameters for in house plasma spray torch

Fixed operating parameters	
Arc current intensity	600 A
Spray torch scan velocity	1 m/s
Variable operating parameters	
Spray distance	20 to 50 mm
Plasma gases mixture	Ar-H_2 (45-15 L/min)
and mass enthalpy	Mass enthalpy = 13.2 MJ/kg
	Ar-He (30-30 L/min)
	Mass enthalpy = 11.5 MJ/kg

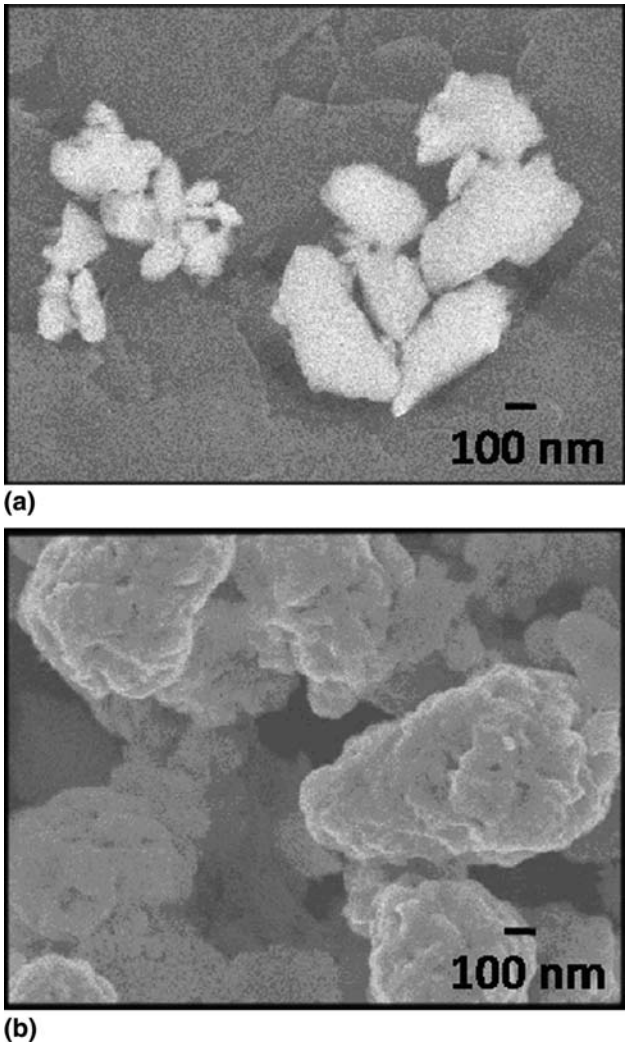

Fig. 2 SPS morphologies of commercial (8YSZ) and synthesized (NiO/8YSZ) powders

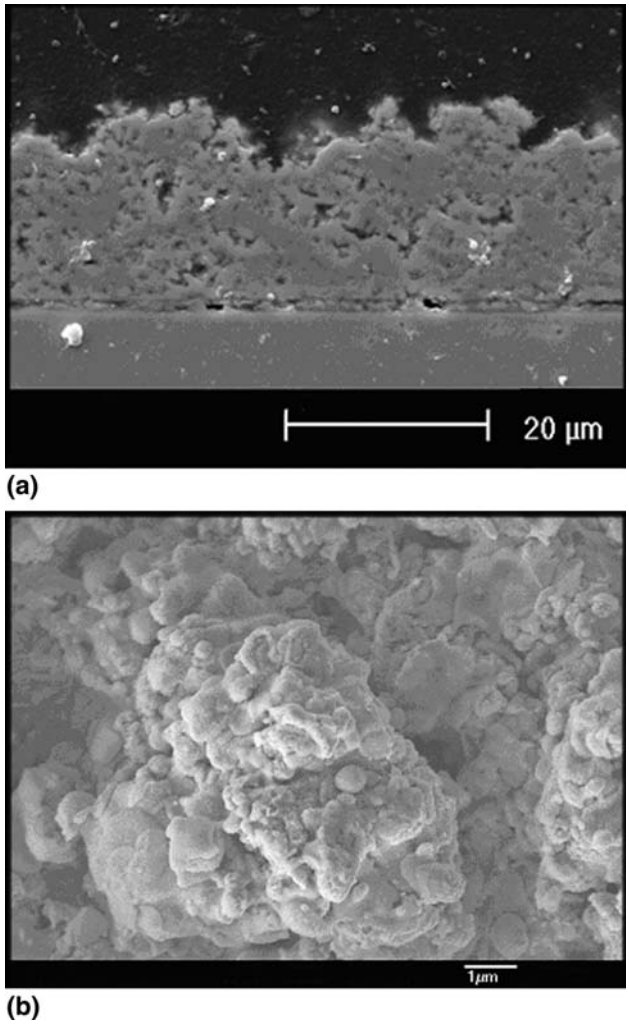

Fig. 3 SPS—NiO/8YSZ layer manufactured at 50 mm with an Ar-H_2 plasma flow: (a) Polished cross section; (b) top view

to the plasma forming gas mixture and power parameters (that is to say according to the plasma flow momentum density and thermodynamic properties and transport coefficients). Indeed, these operating parameters appear critical in SPPS since a chemical precipitation should take place in the time of only a few tenths of millisecond of reaction.

2.5 Substrates

Layers were deposited on polished (i.e., average roughness Ra ~ 0.03 µm and peak-to-valley height Rz ~ 0.3 µm) low-carbon (i.e., 0.1 wt.%) steel substrates and preheated by the plasma flow to about 400 °C. Surface temperature was measured by infrared pyrometry in the 8-14 µm wavelength range.

2.6 Coatings Characterization Techniques

The crystalline phase composition of layers was quantified by x-ray diffraction (XRD) using a Siemens D5000 diffractometer with a back monochromator (Co-Kα radiation, λ = 1.7890 Å). The XRD patterns were collected in a 2θ range from 20° to 80° with a scanning rate of 2°/min.

An environmental scanning electron microscope (SEM, XL30, Philips) and a field emission scanning electron microscope (FESEM, JEOL 7400) were used to characterize the coating microstructures.

DTA-TGA analyses were performed on the precursors mix using a SDT 2960 TGA (TA Instruments, New Castle, DL) system between ambient and 1000 °C in air at atmospheric pressure.

3. SPS Layers

3.1 Composite Powder Characterization

Figure 2 shows the morphology (FESEM) of the synthesized powder particles. NiO covers the 8YSZ grains. This leads to a broader particle size distribution

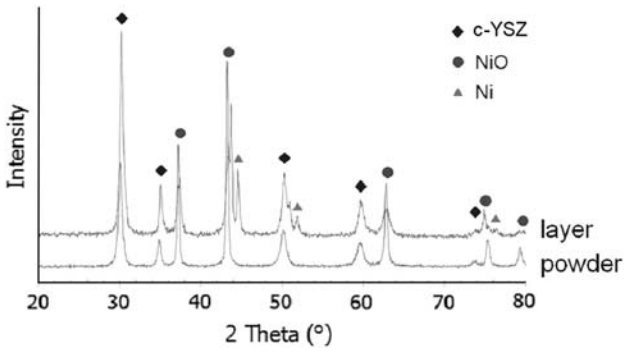

Fig. 4 SPS—XRD patterns of feedstock powder and layers sprayed with an Ar-H_2 plasma flow (mass enthalpy: 13.5 kJ/kg) at 40 mm

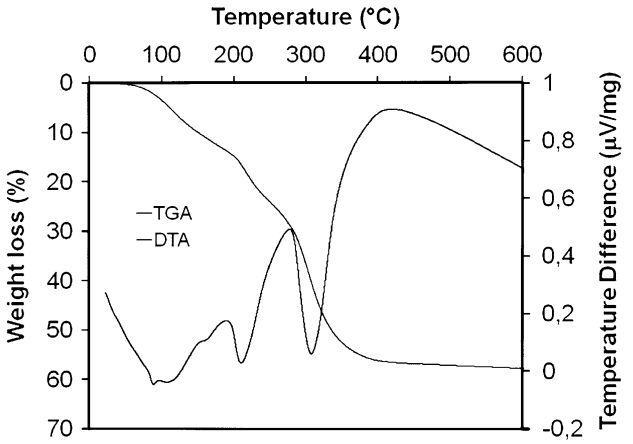

Fig. 5 SPPS—TDA-TGA of mix precursors at a heating rate of 5 °C/min in air at atmospheric pressure

(and a higher average diameter, d_{50}, of about 1400 nm) together with a lower specific surface area compared to the starting 8YSZ powder (7 m^2/g to be compared to 10 m^2/g). In these conditions, even if the nickel oxide and the YSZ seem to be homogeneously dispersed, it appeared very difficult to stabilize this powder in an alcoholic system: large agglomerates and isolated NiO particles sedimented very fast despite of the dispersant. This is very likely due to the powder high specific mass. In order to ease the dispersion of nickel oxide particles within the suspension, dispersion in an aqueous media was experimented but did not prove its efficiency in term of stabilization.

3.2 Microstructure and Phase Composition

The layer manufactured at a spray distance of 40 mm under an Ar-H_2 (45-15 L/min) plasma flow is shown in Fig. 3. Under the considered operating conditions, in particular the fairly low mass load of the suspension, the average deposited thickness per pass is estimated to be

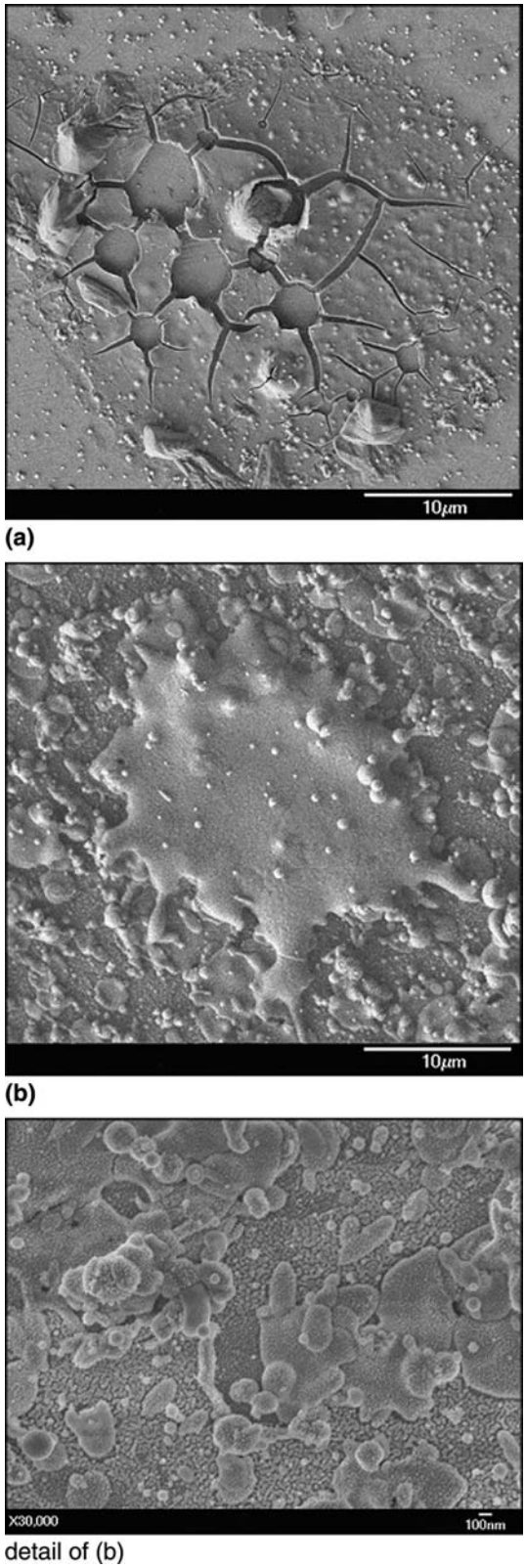

Fig. 6 SPPS—Lamellae/particles collected by single scan experiment from solution precursors at a spray distance of 40 mm with an Ar-H_2 plasma flow: (a) substrate at room temperature; (b) substrate preheated at 400 °C

about 1 μm. Further optimizations would be required to increase this value.

The top surface (Fig. 3b) shows that the layer is principally composed of melted lamellae and untreated or resolidified spherical particles (of average diameter smaller than 1 μm). Micrometer-sized voids are detected in the cross section (Fig. 3a).

The diffraction patterns of the synthesized powder and the layer are shown in Fig. 4. The synthesized powder is only composed of oxides: Y_2O_3/ZrO_2 and NiO. Ni peaks are also detected. Ni results very likely from the reduction of O^- and O^{2-} species by H^+ species resulting from the vaporization/ionization of Et-OH used as liquid phase and from the ionization of H_2 used a secondary plasma forming gas.

4. SPPS Layers

4.1 Physical and Thermal Properties of Solution Precursors

Rheological analyses showed that the solution (with the considered low concentration) exhibits a Newtonian fluid behavior and a viscosity of 6.7×10^{-3} Pa s at ambient temperature (to be compared, for example, to viscosity of pure water of 10^{-3} Pa s at the same temperature). It is evident from the TGA curve that weight loss occurs from 80 to 400 °C (Fig. 5). The DTA curve (Fig. 5) shows that an exothermic reaction occurs first around 100 °C corresponding to the dehydration of the precursors. Dehydration is followed by two endothermic peaks between 300 and 400 °C corresponding to the decomposition and oxidation of precursors, respectively.

4.2 Effect of Substrate Preheating on Lamella Formation

Single pass experiments were carried-out to understand the effect of substrate preheating on layer formation. In single scan experiments, polished substrates mounted on a pendulum passed across the plasma jet at a scan velocity of about 1 m/s to collected individual particles.

Figure 6 shows several typical morphologies of particles collected on substrates at room temperature (Fig. 6a) and preheated (~400 °C) (Fig. 6b). On a substrate kept at room temperature, a combination of solid spheres and aggregates is detected together with flattened lamellae typical of non-pyrolyzed precursors (mud type) upon their impact: the visible cracks result very likely from the shrinkage due to solvent evaporation. On the preheated substrate, a mixture of lamellae and spheres is detected with no evidence of non-pyrolized precursors: pyrolysis ends very likely at the substrate surface due to its temperature of 400 °C. The lamellae results from molten particles which spread and flatten forming features of equivalent diameters ranging from 1 to 10 μm whereas the spheres result very likely from particles which resolidified during their flight due to their small size and form features of average diameters smaller than 1 μm. Xie et al. (Ref 13) made the same observations on a substrate kept at room temperature where non-pyrolized precursor was detected (but only on the spray bead edges). On a preheated substrate, lamellae and solid spheres were also present only in the spray bead central part.

At higher magnification (Fig. 6b), lamellae (molten particles when impacting the substrate) and near spherical nano-sized particles with a typical dimension of 50 nm (resolidified particles when impacting the substrate) are detectable, themselves being constituted by the agglomeration of nano-sized particles of even smaller sizes, in the order of a few nanometers.

The fairly large size distribution of these features (several orders of magnitudes) results very likely from heterogeneities in solution stream fragmentation mostly due to plasma fluctuations induced by arc root fluctuations depending themselves upon power parameters and plasma gas mixture.

4.3 Phase Composition

Figures 7 and 8 display the phase constituents present in the layers for different spray distances (20 to 50 mm) for the two plasma gases mixtures (Ar-H_2 and Ar-He). No differences were found between preheated substrates and substrates kept at room temperature prior spraying. Very likely, the high heat flux imparted by the plasma to the substrate during coating formation lead to its fast heating with transient temperatures well above 400 °C (preheating temperature), leading to the pyrolysis of non-pyrolized precursors at the substrate surface. Results depicted hereafter refer to spray conditions where substrates were preheated to 400 °C prior spraying.

Whatever the considered spray operating parameters, cubic YSZ and NiO peaks are detected in diffraction patterns. The presence of Ni can be also detected until a critical spray distance depending upon the plasma gas mixture (and hence the plasma mass enthalpy) and their reactivity. As previously stated in section 3.2, Ni results very likely from the reduction of O^- and O^{2-} species by H^+ species resulting from the vaporization/ionization of Et-OH used as solvent and, when considering Ar-H_2 plasma gas mixture, also from the ionization of H_2. Indeed, under an Ar-H_2 plasma flow, Ni is detected until a spray distance of about 40 mm against 30 mm only under an Ar-He plasma flow. Whatever the plasma gas mixture, Ni particles oxidize after these critical distances very likely due to oxygen species from the surrounding atmosphere entrapped in the plasma flow. Additional studies should be undertaken to further address this point.

Beside, it is well known that the range of solid solubility in both binary and ternary zirconia systems is very wide. A single phase cubic solid-solution ZrO_2-CaO-NiO is referenced in the literature (Ref 23) with ZrO_2 varying from 86 to 48 mol.%, NiO from 5 to 30 mol.%, and CaO from 2 to 22 mol.%. Authors have been unable to identify in the literature existence of an analogous solid-solution in the ZrO_2-Y_2O_3-NiO system. Moreover, AO and B_2O_3 oxides form very often spinels. Authors have been also unable to identify in the literature if the NiY_2O_4 spinel could form

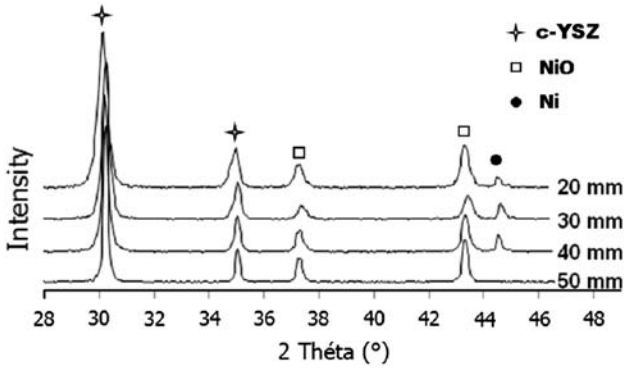

Fig. 7 SPPS—XRD patterns of layers sprayed with an Ar-H_2 plasma flow (mass enthalpy: 13.2 kJ/kg) at different spray distances

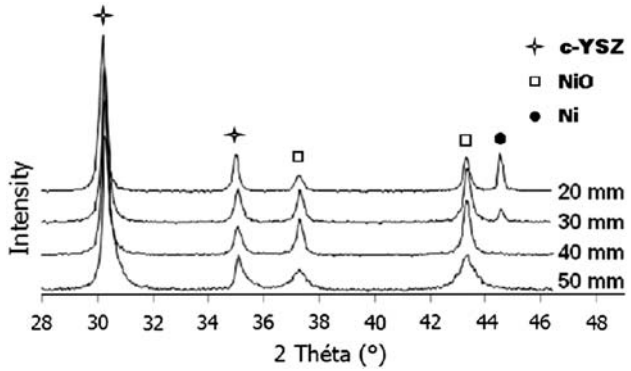

Fig. 8 SPPS—XRD patterns of layers sprayed with an Ar-He plasma flow (mass enthalpy: 11.5 kJ/kg) at different spray distances

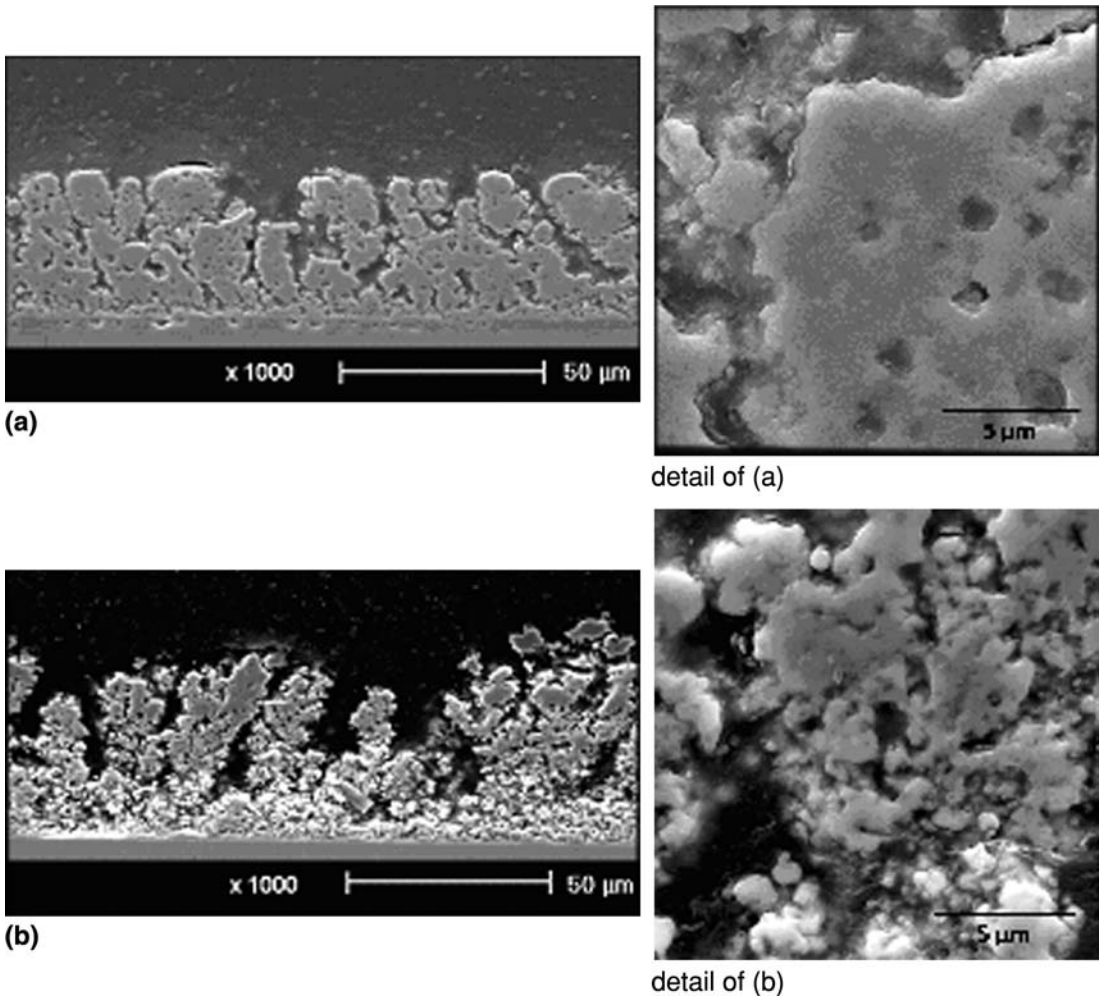

Fig. 9 SPPS—Polished cross sections of layers manufactured with different processing parameters: (a) 20 mm spray distance and Ar-H_2 gas mixture; (b) 50 mm spray distance and Ar-H_2 gas mixture; (c) 20 mm spray distance and Ar-He gas mixture; (d) 50 mm spray distance and Ar-He gas mixture

(and which would be the thermodynamic conditions) from the ternary ZrO_2-Y_2O_3-NiO system. No evidence of this phase was identified on the XRD patterns but a more focused study should be undergone to address this specific and important point by coupling, for example, HR-TEM with HR-XRD analyses.

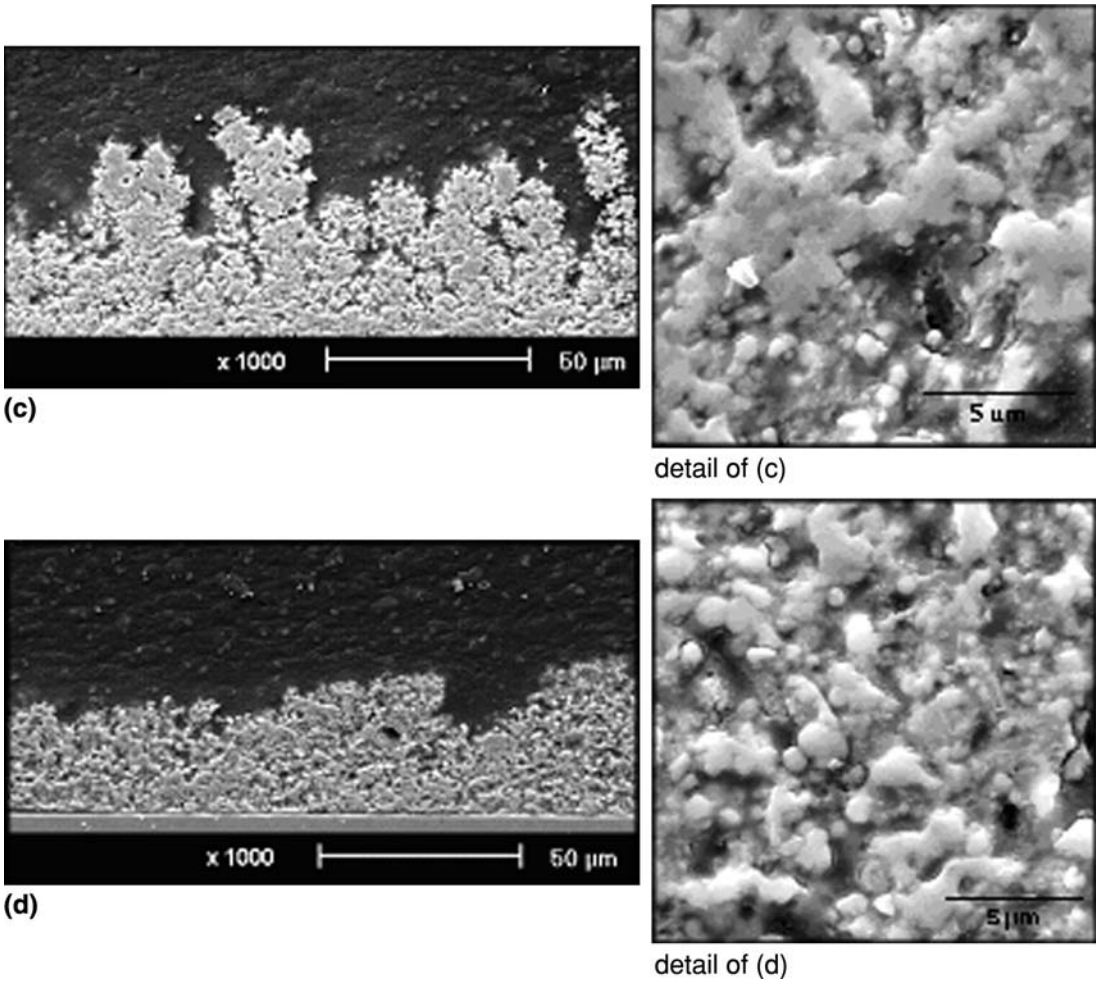

Fig. 9 Continued

At a spray distance as short than 20 mm, a small shift of about 0.4° of the YSZ peaks can be observed. This shift is very likely due to an incomplete reaction between ZrO_2 and Y_2O_3 at such a short spray distance (and hence reaction time). In this specific case, the Y_2O_3 content of the cubic phase is hence lower than the expected 8 mol.%.

4.4 Microstructure

Figure 9 shows polished cross sections of layers manufactured at 20 and 50 mm under Ar-H_2 and Ar-He plasma flows. Under the considered operating conditions, in particular the fairly low solution concentration, the average deposited thickness per pass is estimated to be about 0.6 µm. Increasing this deposition efficiency will require obviously further optimizations.

The superimpositions of spread beads to form a pass and of passes to form the layer make it difficult to distinguish the specific features depicted in section 4.2, in particular flattened lamellae. Moreover, the higher interaction time between the substrate and the high heat flux imparted by the plasma flow during layer formation compared to spray bead formation leads to a higher thermal load that could induce some additional mechanisms such as fast sintering, local remelting, etc.

Once again, no structural differences were found between preheated substrates and substrates kept at room temperature prior spraying, very likely for the same reason than the one presented in section 4.3 and results depicted hereafter refer also to spray conditions where substrates were preheated to 400 °C prior spraying.

It can be observed in the case of an Ar-H_2 plasma flow that more features (voids, stacking defects, etc.) are present in the layers and that the particles have the tendency to agglomerate or aggregate together to create columnar porous architectures. These features develop because of the fluctuations of the Ar-H_2 plasma jet that impedes a homogeneous processing of the solution. Those fluctuations result from the electric arc root fluctuations (i.e., restrike operating mode characterized by a $\Delta V/V$ ratio of about 1) that are emphasized by the presence of molecular gas in the plasma gas mixture. In the case of an Ar-He plasma flow, the coating is denser at a 50 mm spray distance than at 20 mm. The increase in

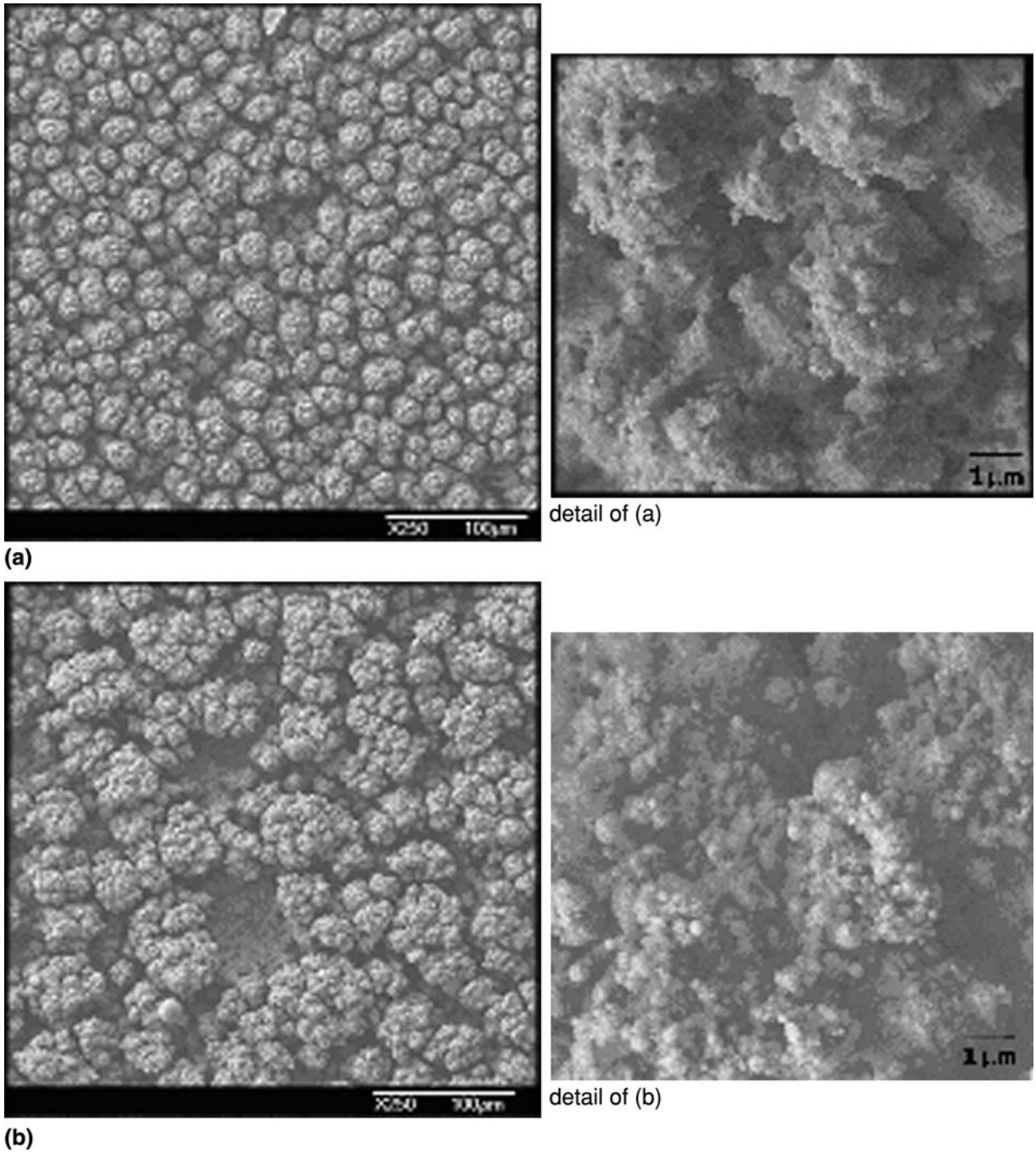

Fig. 10 SPPS—Surface of the layers under different processing parameters: (a) 20 mm spray distance and Ar-H_2 gas mixture; (b) 50 mm spray distance and Ar-H_2 gas mixture; (c) 20 mm spray distance and Ar-He gas mixture; (d) 50 mm spray distance and Ar-He gas mixture

the spray distance permits very likely to induce a more complete treatment of the particles (pyrolysis for example can be completed) into the plasma jet and consequently a denser coating. The layer structures are constituted of dense areas and spherical resolidified particles (<1 µm). The resolidified particles are more numerous at 50 mm than 20 mm and under an Ar-H_2 plasma flow compared to an Ar-He one.

Figure 10 displays the top view of the layers for the same operating parameters as the cross sections depicted in Fig. 9. The top views show that the coatings are porous and made of rather big agglomerates. On the detail views it can be evidenced once again that the higher the spray distance, the more numerous the resolidified particles.

Contrary to SPS process where injection problems associated to dispersion and stabilization of the powder in

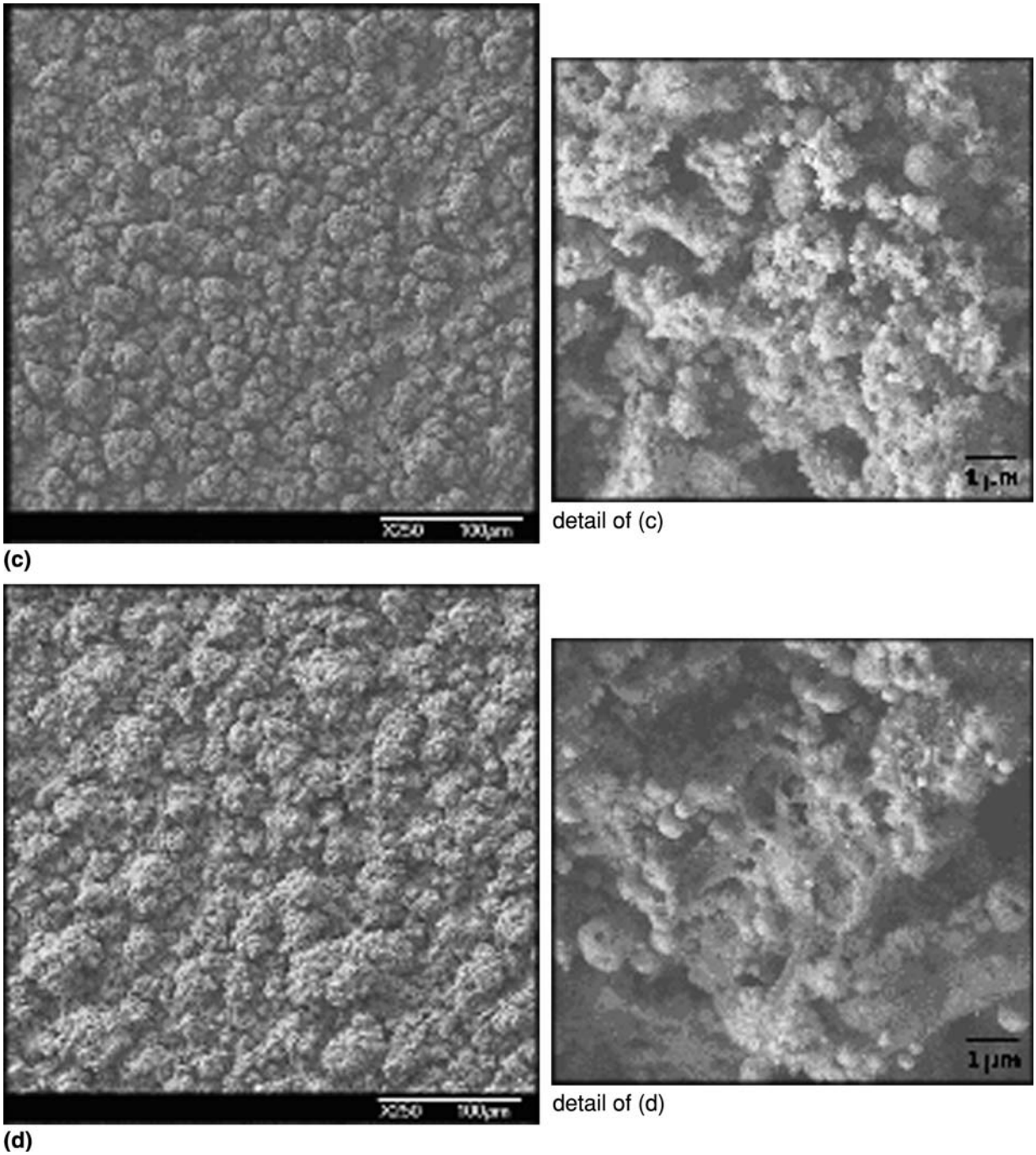

Fig. 10 Continued

the solvent have to be resolved, SPPS permits an intimate mixing between the three nitrate salts in the solution.

The hypothesis of a more homogeneous dispersion of NiO in YSZ can be made. To confirm this hypothesis, a cross section of a layer sprayed under an Ar-He plasma gas mixture at a 50 mm spray distance was observed by SEM in backscattered electrons mode (BSE) and EDS maps were collected for each constituting elements (Ni, Y, and Zr), as shown in Fig. 11. From these maps, it can be seen that the nickel element, representing in most cases the corresponding oxide, is homogeneously dispersed into the matrix. Changing operating parameters does not modify the homogeneous distribution of oxides in each other.

5. Conclusion

The results presented in this work demonstrate that structured NiO/8YSZ layers can be formed by SPS and SPPS. For the two routes, a homogeneous distribution of

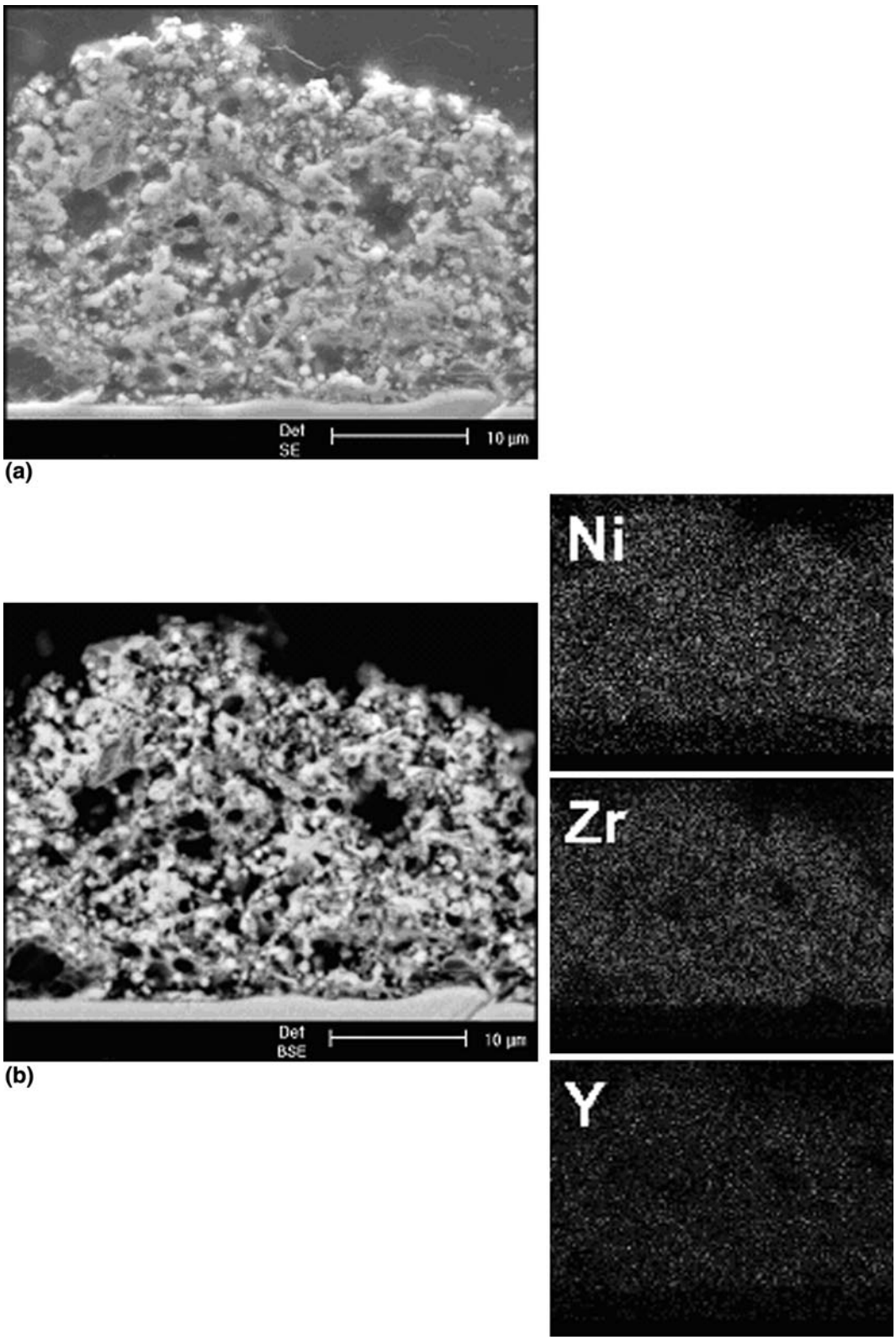

Fig. 11 SPPS—Cross section of the layer and elemental distribution maps for Ni, Y, and Zr at a spray distance of 50 mm with an Ar-He plasma flow (mass enthalpy: 11.5 kJ/kg): (a) scattered electron (SE) mode; (b) backscattered electron (BSE) mode

NiO in the YSZ matrix is observed. Nevertheless, SPS presents some issues regarding the poor stability and fast sedimentation of the suspension due to the high specific mass of the powder. The average deposited thicknesses per pass were estimated to be about 1 μm for SPS and 0.6 μm for SPPS, to be compared to 10 to 30 μm deposited per pass when considering conventional APS process and an oxide feedstock. Those values do not represent maximal values that can be reached with this type of plasma torch and deposition efficiency will have to be optimized in further studies.

SPPS is a good alternative to circumvent poor stability and fast sedimentation of the suspension. It offers also a more important flexibility to tailor layer composition and structure (i.e., void content, surface area, connectivity, etc.). The mix of solutions fragmented into droplets where nickel, zirconium, and yttrium salts are intimately mixed permits to manufacture layers exhibiting a very fine structure with features exhibiting characteristic dimensions well below 1000 nm. The plasma mass enthalpy and the spray distance have predominant effects on the chemical species in-flight pyrolysis.

The plasma gas mixture has also an impact on the void content of the layers. Considering plasma flows with a high fluctuation level (Ar-H_2), the fragmentation of the liquid by the jet is heavily disturbed and the layer is more porous than with an Ar-He plasma flow leading to lower plasma flow fluctuations. Moreover, the plasma gas mixture has an effect on the composition of the layer regarding the oxidation state of the nickel.

Further works should be focused on the better understanding of coating formation mechanisms, in particular the effect of the high thermal flux imparted by the plasma to the substrate, on the quantification of the coating structure and its electrochemical properties.

Acknowledgments

This work is granted by French ANR PRODHYGE consortium (CEA, AREVA, ARCELOR-MITAL, LMP—University of Bordeaux, SPCTS—University of Limoges) under Grant No. ANR-PANH-06-013-05, the financial support of which is gratefully acknowledged.

References

1. M.-F. Han, H.-Y. Yin, W.-T. Miao, and S. Zhou, Fabrication and Properties of Anode-supported Solid Oxide Fuel Cell, *Solid State Ionics*, 2008, **179**, p 1545-1548
2. H. Kassner, R. Siegert, D. Hathiramani, R. Vassen, and D. Stoever, Application of Suspension Plasma Spraying (SPS) for Manufacture of Ceramic Coatings, *J. Therm. Spray Tech.*, 2008, **17**(1), p 115-123
3. A.R. Nicoll, A. Salito, and K. Honegger, The Potential of Plasma Spraying for the Deposition of Coatings on SOFC Components, *Solid States Ionics*, 1992, **1-2**(152), p 269-275
4. S. Kim, O. Kwon, S. Kumar, Y. Xiong, and C. Lee, Development and Microstructure Optimization of Atmospheric Plasma-Sprayed NiO/YSZ Anode Coating for SOFCs, *Surf. Coat. Technol.*, 2008, **202**, p 3180-3186
5. R. Vaßen, D. Hathiramani, J. Mertens, V.A.C. Haanappel, and I.C. Vinke, Manufacturing of High Performance Solid Oxide Fuel Cells (SOFCs) with Atmospheric Plasma Spraying (APS), *Surf. Coat. Technol.*, 2007, **202**, p 499-508
6. O. Marchand, R. Rampon, G. Bertrand, and C. Filiatre, How Long is the Way to Manufacture Solid Oxide Fuel Cells with Suspension Plasma Spraying? *International Thermal Spray 2008: Thermal Spray Crossing Borders*, E. Lugscheider, Ed., June 2-4, 2008 (Maastricht, The Netherlands), DVS, 2008, p 571-575
7. H. Cangul, L. Broday, K. Salnikow, J. Sutherland, W. Peng, Q. Zhang, V. Poltaratsky, H. Yee, M.A. Zoroddu, and M. Costa, Molecular Mechanisms of Nickel Carcinogenesis, *Toxicol. Lett.*, 2002, **127**, p 69-75
8. P. Fauchais, V. Rat, J.-F. Coudert, R. Etchart-Salas, and G. Montavon, Operating Parameters for Suspension and Solution Plasma-Spray Coatings, *Surf. Coat. Technol.*, 2008, **202**, p 4309-4317
9. D. Chen, E.H. Jordan, and M. Gell, Effect of Solution Concentration on Splat Formation and Coating Microstructure using the Solution Precursor Plasma Spray Process, *Surf. Coat. Technol.*, 2008, **202**, p 2132-2138
10. N.P. Padture, K.W. Schlichting, T. Bhatia, A. Ozturk, B. Cetegen, E.H. Jordan, M. Gell, S. Jiang, T.D. Xiao, P.R. Strutt, E. Garcia, P. Miranzo, and M.I. Osenti, Towards Durable Thermal Barrier Coatings with Novel Microstructures Deposited by Solution Precursor Plasma Spray, *Acta Mater.*, 2001, **49**, p 2251-2257
11. L. Xie, X. Ma, E.H. Jordan, N.P. Padture, D.T. Xiao, and M. Gell, Identification of Coating Deposition Mechanisms in the Solution-Precursor Plasma-Spray Process using Model Spray Experiments, *Mater. Sci. Eng. A*, 2003, **362**, p 204-212
12. L. Xie, X. Ma, A. Ozturk, E.H. Jordan, N.P. Padture, B.M. Cetegen, D.T. Xiao, and M. Gell, Processing Parameter Effects on Solution Precursor Plasma Spray Process Spray Patterns, *Surf. Coat. Technol.*, 2004, **183**, p 51-61
13. E.H. Jordan, L. Xie, X. Ma, N.P. Padture, B. Cetegen, A. Ozturk, J. Roth, T.D. Xiao, and P.E.C. Bryant, Superior Thermal Barrier Coatings Using Solution Precursor Plasma Spray, *J. Therm. Spray Tech.*, 2004, **13**(1), p 57-65
14. T. Fukui, S. Ohara, M. Naito, and K. Nogi, Synthesis of NiO-YSZ Composite Particles for an Electrode of Solid Oxide Fuel Cells by Spray Pyrolysis, *Powder Technol.*, 2003, **132**, p 52-56
15. J. Karthikeyan, C.C. Bernt, J. Tikkanen, S. Reddy, and H. Herman, Plasma Spray Synthesis of Nanomaterial Powders and Deposits, *Mater. Sci. Eng. A*, 1997, **238**, p 275-286
16. P. Fauchais, R. Etchart-Salas, C. Delbos, M. Tognonvi, V. Rat, J.-F. Coudert, and T. Chartier, Suspension and Solution Plasma Spraying of Finely Structured Layers: Potential Application for SOFCs, *J. Phys. D Appl. Phys.*, 2007, **40**, p 2394-2406
17. K.W. Schlichting, N.P. Padture, E.H. Jordan, and M. Gell, Failure Modes in Plasma-Sprayed Thermal Barrier Coatings, *Mater. Sci. Eng. A*, 2003, **342**, p 120-130
18. L. Xie, D. Chen, E.H. Jordan, A. Ozturk, F. Wu, X. Ma, B.M. Cetegen, and M. Gell, Formation of Vertical Cracks in Solution-Precursor-Sprayed Thermal Barrier Coatings, *Surf. Coat. Technol.*, 2006, **201**, p 1058-1064
19. Y. Wang and T.W. Coyle, Optimization of Solution Precursor Plasma Spray Process by Statistical Design of Experiment, *J. Therm. Spray Tech.*, 2008, **17**(5-6), p 692-699
20. S.T. Aruna, M. Muthuraman, and K.C. Patil, Synthesis and Properties of Ni-YSZ Cermet: Anode Material for Solid Oxide Fuel Cells, *Solid State Ionics*, 1998, **111**, p 45-51
21. S. Li, R. Guo, J. Li, Y. Chen, and W. Liu, Synthesis of NiO-ZrO_2 Powders for Solid Oxide Fuel Cells, *Ceram. Int.*, 2003, **29**, p 883-886
22. M. Marinsek, K. Zupan, and J. Maeek, Ni-YSZ Cermet Anodes Prepared by Citrate/Nitrate Combustion Synthesis, *J. Power Sources*, 2002, **106**, p 178-188
23. H.M. Ondik and H.F. McMurdie, *Phase Diagrams for Zirconium and Zirconia Systems*, The American Ceramic Society, Westerville, OH, USA, 1998, p 184